Full-field monitoring methods for damage analysis on aeronautical CFRP specimens under fatigue loads

Full-field monitoring methods for damage analysis on aeronautical CFRP specimens under fatigue loads

R Nobile[1], F W Panella[1], A Pirinu[1*] and A Saponaro[1]

[1]University of del Salento, Department of Engineering for Innovation, Viale per Monteroni, Lecce (LE), 73100, Italy

[*]alessandra.pirinu@unisalento.it

Abstract. The present paper is focused on full-field experimental monitoring procedures to be employed during HCF fatigue testing on two series of CFRP open hole samples. Two different experimental methodologies based on thermographic techniques and displacement measurements with Digital Image Correlation (DIC) analysis are employed for damage settlement and evolution to be detected up to failure, together with correspondent compliance analysis. Combined monitoring approaches, based on thermo-elastic and dissipative phenomena, together with stiffness properties variations, are claimed to offer precise damage state localization during tests in real time; in addition, DIC analysis is performed during low-frequency fatigue cycle is studied for better failure prediction and damage location. The thermal parameters and experimental compliance correlation seem to indicate similar signal variation during damage progress and after proper data elaboration; contemporaneous raw thermal measurements in critical zones of specimens under fatigue life offer a kind of delamination recognition at specific layer interface and location, as well as propagation before final failure. Sample under tensile load on the other hand reveal delaminations indirectly on the surface. In addition, non-destructive thermographic and ultrasound tests are performed at regular intervals during fatigue life.

Keywords: CFRP, damage prediction, delamination, DIC, Fatigue, TSA.

1. Introduction

Composite structures showed a growing employment in aerospace and automotive field due to their elevated mechanical properties, such as strength-to-weight and stiffness-to-weight ratios in case of Carbon fiber-reinforced polymers (CFRP), as well as improved challenging geometries to be achieved with advanced manufacturing and elevated fatigue resistance in comparison to classical metallic alloys [1]. However, the non-homogeneous behaviour and different interface conditions with other parts seem to exhibit critical mechanical response behaviour, showing a continuous degradation of mechanical properties before the final structural failure with alternate stressed during service life [2].

The detection and prevention of damage evolution, employing a no-contact and less expensive monitoring technique represents an ongoing challenge for the Structural Health Monitoring (SHM) of composite aircraft parts under fatigue with relatively high frequency levels [3, 4]. Non-Destructive Inspections (NDIs) and preventive replacement are required by the scheduled maintenance program to ensure stable and reliable operating condition during service life, involving consequent considerable costs. Among the different SHM techniques, optical and non-contact ND methods such as Thermoelastic

Stress Analysis [5] (TSA) and Digital Image Correlation [6] (DIC) seem to provide the full-field stress states and damage induced effects of monitored structures [1]. Several authors demonstrate the damage evolution analysis, employing the Infrared Thermography (IRT), which provides a real-time continuous monitoring procedure on inspected elements under cyclic loads, unlike the local assessing of strain gauges. Thermoelastic stress analysis (TSA) is a non-contact sub-surface technique based on the thermoelastic effect which correlate the stress distribution to temperature variations detected in inspected component subjected to cyclic loads employing a sensitive infrared camera [1, 5]. Therefore, recent researches highlight the damage detection capability and monitoring potentials of micro-bolometric infrared camera showing the more cost effective and commercial availability solutions for TSA approach without an expensive thermographic equipment [7, 8].

In this work, two different Carbon Fiber/epoxy (CFRP) composite specimens in the form of Flat Open Hole laminated elements are tested under tension-tension cyclic loading, realized in pre-preg autoclave curing or through the Liquid Resin Infusion technology, to study fatigue behaviour in presence of hole.

Experimental tests are in-real time monitored with thermal acquisitions, exporting reveal effects of localized tensile loads and notched zones as source of delamination initiation, whilst delamination growth is experimentally investigated before failure and correlated to fatigue residual life expectancies. However, the present proposed work efforts consist of better damage localization (well observed with visual and thermographic inspection) and quantification of propagation severity, compared with the well-established compliance analysis. Continuous damage accumulation is monitored with infrared thermal camera and DIC measurements at specified intervals during fatigue life, coupled with mechanical stiffness degradation during whole fatigue life for CFRP elements after High Cycle fatigue (HCF) loading.

2. Materials and Methods

2.1. CFRP elements and experimental procedures

Both sample series are CFRP composites in Figure 1(a) in Flat Open Hole configuration, and all static and cyclic tests are performed in load control mode on the servo - hydraulic INSTRON 8850 axial-torsion test machine, equipped with a load cell of ± 250 KN and governed by a computer equipped with INSTRON WAVE MATRIX software.

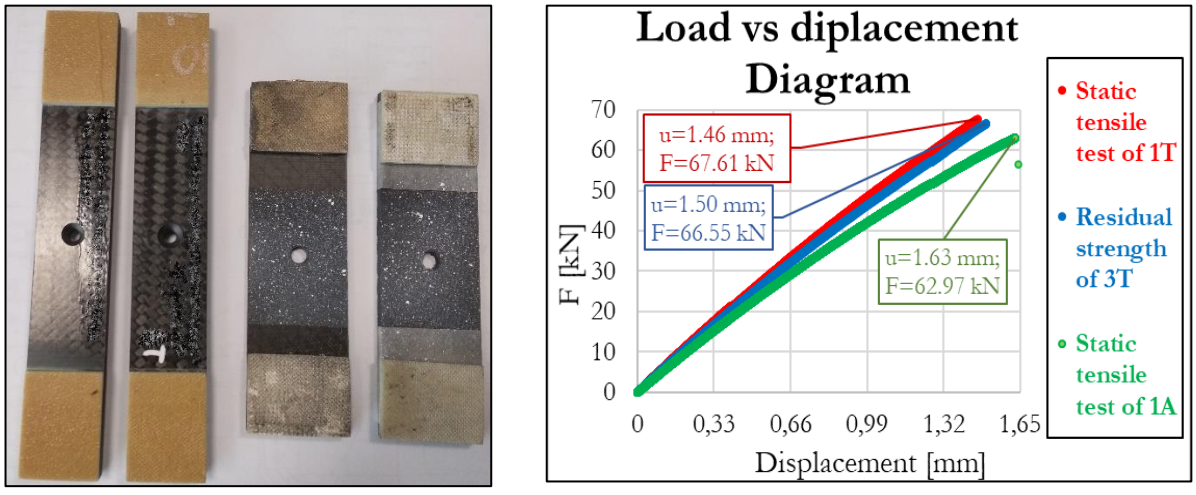

(a) (b)

Figure 1. (a) Example OHT specimens of 'T-S' (left) and 'A' (right) series; (b) load-displacement diagram for OHT series.

The first batch (denotated 'T-S' type) consist of flat samples [Dim. 177.8 × 28.8 × 6.55 mm] with a central hole of 4.74 mm with countersink 2 × 45°, realized in autoclave of composite, aided to reproduce

tensile fatigue behaviour in presence of hole for aeronautic bolted junctions. These specimens consist of 20 woven fabrics of thickness 0.327 mm with a stacking sequence of [±45, 0/90, 0/90, 0/90, ±45]2s symmetrically arranged.

The second case of study includes two CFRP elements [Dim. 130 × 39 × 6.78 mm] with a flat central hole of 6 mm, denotated as 'A-type' samples, laminated with unidirectional layers in a specific layup $[+45, -45, 0, +90]_{2s}$ symmetrically arranged in angle-ply configuration of 16 plies, manufactured through Liquid Resin Infusion process.

For both OHT batches, two preliminary static tests are done for assessing the reference ultimate tensile strengths (UTS), to establish subsequent cyclic loads level. Figure 1(b) shows example diagrams of static test for each series, where an average maximum static load (F_{static}) of 67.61 kN and 62.97 kN have been measured for 'T-S' samples and of 'A' specimens, respectively. Successively, three 'T-S'-type specimens and two 'A'-type samples are tested HCF selecting specific load levels, test parameters and resulting data scheduled in Table 1 in terms of endurance.

The static and cyclic tests follow the standard practices ASTM D5766 M for open-hole tensile strength and ASTM D7615 M for open-hole fatigue response of polymer matrix composite laminates, respectively. The fatigue tests are conducted on CFRP samples at a frequency load of 9 Hz employing R = 0.1 as load ratio under sinusoidal waveform. In Table 1, fatigue parameter F_{max_norm} represents the normalized maximum load percentage of each fatigue test and damaged zones and failure modes are displayed in each CFRP series with similar aspect, as shown in Figure 2(a).

Table 1. Experimental fatigue tests for 'A' and 'T-S' OHT series.

Sample batch	ID fatigue sample	Stress ratio (*R*)	Load frequency [Hz]	F_{max_norm} [%]	Number of cycles (N_f)	*Damage zone and type*
'A' Series	A2	0.1	9	87.33	204050	Crack at 1st and delamination at 8th ply
	A3			79.39	126225	Crack at 1st and delamination at 8th ply
'T-S' Series	3T			85.00	Stop at 10^6	Undamaged
	4T			91.66	737481	Crack and delamination around countersunk layers
	5T			93.88	318797	Crack and delamination around countersunk layers

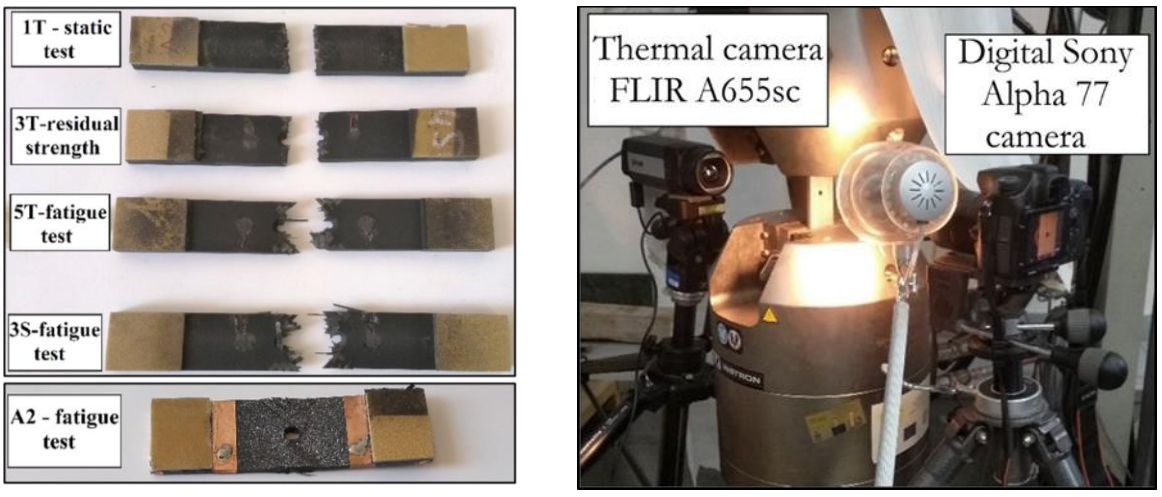

(a) (b)

Figure 2. (a) Example of damaged samples of 'T-S' and (b) 'A' series; (b) experimental and monitoring setup of OHT samples for fatigue damage evaluation with IR and optical cameras.

In the 'T-S' series, delamination initiations, matrix cracking and finally fibre breakage are observed through fatigue cycle, in the layers at the onset of the countersunk region, while the shear cracks at 45°

to fibre directions on 1st and 16th layers with delamination observed in 'A' series during cyclic loading, with central ply delamination observed in the final stages.

A residual strength test is carried out on the undamaged 3T after fatigue loads and similar load-displacement trends and damage modes are detected for static 1T and 3T samples, as shown in Figures 1 (b) and 2 (a). In fatigue test, the specimen stiffness variation is commonly employed to express the damage state of polymer composites [9] and a cumulative damage D_K parameter is defined as [10]:

$$D_K = \left[1 - \frac{K}{K_0}\right] * 100 \quad (1)$$

where K and K_0 represent the actual and initial stiffnesses, respectively. The experimental results include the compliance analysis where the stiffness behaviour is evaluated during all fatigue life until final failure.

2.2. Damage monitoring and inspection procedures

A monitoring strategy consists of thermographic and digital image correlation acquisitions to evaluate damage initiation and progression during cyclic loading. Specimens are positioned inside the test machine clamps and monitored at regular intervals with a micro-bolometric infrared thermal camera and digital high-resolution camera, as shown in the setup of Figure 2(b).

The FLIR A655sc thermal camera is employed, equipped with an uncooled vanadium oxide micro-bolometer detector that provides 14-bit data up to 50 frames per second. For each CFRP elements, thermal signals are recorded at regular intervals of 5000 cycles as a function of the expected fatigue life with a frame of 640 × 240 pixels, using a frame rate of 100 Hz and observation time of 10s, in controlled environment temperature between 23÷26 °C. The thermal camera is MATLAB compatible and controlled by a computer equipped with the Research-IR software, with which the thermal sequences are acquired and converted in '.mat' or '.csv' file for the post processing analysis.

According to thermoelastic theory, the temperature change between the peak and valley of the cyclic load on an orthotropic material could be correlated to the stress change in an adiabatic environment following the Equation [10]:

$$\frac{\Delta T}{T} = -\frac{1}{\rho * C_p} \sum_{k=1}^{3} \alpha_k * \Delta\sigma_k \quad (2)$$

Where ΔT [K] represents the temperature oscillation and T [K] is the absolute temperature at the mean load level on inspected specimen under fatigue loading, ρ [kg/m^3] the material density, C_p [J/(kg*K)] is the specific heat capacity at constant pressure, α_k [K^{-1}] represents each directional coefficient of thermal expansion (CTE), and $\Delta\sigma_k$ represents the amplitude of the principal stresses [1, 10]. The ratio $\alpha_k/(\rho * C_p)$ is denotated as thermoelastic constant.

As demonstrated by different authors [1, 10], thermal dissipation could be related to damage progression and TSA based approach could be successfully employed as an indicator of damage accumulation during fatigue loading. During low frequency fatigue test, the average temperature of sample seems to increase with cycles, as illustrated in Figure 3(b). Thermal variation in terms of amplitude oscillation is related to reversible thermoelastic heating and cooling during cycling loads [10]. Therefore, when the material becomes deformed or damaged, the material volume always followed by heat releases and a part of energy necessary to damage propagation transformed in an irreversible heat source [11]. Since, both the damage initiation and damage propagation up to final failure result extremely difficult to accurately detect with TSA approach, still widely used for rapid fatigue limit estimation tests [13]. In fact, several authors proposed different thermoelastic approaches successfully applied for rapid estimation of the fatigue limit of homogeneous or orthotropic materials in stepwise cyclic tests with increasing stress amplitude levels [12 - 16].

In previous works [20, 22], the authors employed an alternative TSA analytical model proposed by Galietti et al. [13, 23] to extract thermal signal information from thermographic sequences acquired

during each fatigue test. In particular, the thermal signal is processed in the time domain based on the following equation implemented in MATLAB [30]:

$$T(i,j,t) = T_0 + bt + T_{the} * \sin(\omega * t + \pi + \varphi) + A * cos(2 * \omega * t + \psi) \quad (3)$$

Where the sum $T_0 + b * t$ (denotated as T_{sum}) describes the mean increase in the average dissipative thermal signal during fatigue test; ω is the angular frequency with which the imposed load signal varies; T_{the} and φ are respectively the amplitude and the phase of first harmonic component related to thermoelastic signal; A and ψ represent respectively the second component amplitude and the phase of thermal signal obtained at a double frequency [16, 23]. Algorithm allow to extract the various signal information from each selected ROI to obtain as output six (T_0, b, T_{the}, A, φ and ψ) signal parameter reported in equation (3), evaluated during fatigue tests.

The aim of this study consists of a different damage fatigue correlation evolution, introducing TSA contrast parameters based on reversible and irreversible thermoelastic sources. In fact, different methods are proposed in case of ND control thermographic inspections to provide enhancing contrast for defect detection and to reduce various noises and other error sources [17, 18].

Thermal processing techniques lie in thermal contrast evaluation, comparing relative temperature behavior during observation time in selected Regions of Interest (ROIs) in different defective and defect-free zones [18]. In this work, the research focus lies on the possible introduction of a TSA contrast-based method for the cumulative damage identification and quantification in an established zone. The first term of Equation (2) could be combined to evaluate a first normalized Thermoelastic Contrast parameter for specific damage evaluation from reversible heating source during the fatigue life (N_{tot}) as:

$$D_{rev}(N) = \left[\left(\frac{\Delta T}{\bar{T}} - \left(\frac{\Delta T}{\bar{T}}\right)_0\right)\Big/\left(\frac{\Delta T}{\bar{T}}\right)_0\right]_d - \left[\left(\frac{\Delta T}{\bar{T}} - \left(\frac{\Delta T}{\bar{T}}\right)_0\right)\Big/\left(\frac{\Delta T}{\bar{T}}\right)_0\right]_i = \left[\frac{\Delta T}{T}\Big/\left(\frac{\Delta T}{T}\right)_0\right]_d - \left[\frac{\Delta T}{T}\Big/\left(\frac{\Delta T}{T}\right)_0\right]_i \quad (4)$$

Where $\left(\frac{\Delta T}{T}\right)_d$ and $\left(\frac{\Delta T}{T}\right)_i$ represent the TSA ratio of Eq. (1) for damaged and undamaged regions (ROIs) at a given time of fatigue life (N/N_{tot}), normalized with respect to the same relative TSA ratio at initial fatigue life, respectively. The aim of this parameter is the analysis of a damage evolution associated to temperature oscillation and normalized to actual temperature and referred to undamaged reference zone.

In addition, assuming initially undamaged conditions, the cumulative damage zone elated to dissipative heat release could also provide interesting information on material degradation. The authors propose an alternative damage analysis coefficient to the previous one, to be evaluated in function of fatigue life (N/N_{tot}) with a second parameter:

$$D_{diss}(N) = \left[\frac{T - T_0}{T_0}\Big|_d - \frac{T - T_0}{T_0}\Big|_i\right] = \left[\frac{T}{T_0}\Big|_d - \frac{T}{T_0}\Big|_i\right] * 100 \quad (5)$$

Where the TSA parameter D_{diss} represents damage progression associated with a normalized contrast evaluated with temperature ratio of the mean load level in selected damaged and undamaged zones respectively. Therefore, preliminary thermal analysis consists of a suitable selection of proper damaged and undamaged zones in the raw temperature images. Then, in the second processing phase, each sequence of 3D thermal ROIs is post-processed in MATLAB environment following Equations (4) and/ or (5) as function of fatigue life and compared with stiffness behaviour.

For each OHT specimen, the authors optimize experimental monitoring setups to achieve a suitable ROI of the most critical zones where interesting thermal data, displacement fields and in-situ deformations could arise, as illustrated in Figures 2(b) and 3(a) with selected regions of interest (ROIs) on reduced section. The reference intact zones are selected calculated in several ROIs without recorded

significative variations on the proposed damage factors. Since, the damage presented multiple defective spots due to widespread delamination, therefore the authors considered only the defective ROIs close to the hole.

Both sample surfaces are preventively prepared to create the proper pattern with a high random contrast for DIC analysis employing on one side of acrylic paint and with high-temperature black paint for thermal analysis on the opposite one. In Figure 1 (a), an example of surface preparation for DIC analysis is reported for 'A' type samples.

During static and fatigue test, a Digital Sony Alpha 77 camera with macro lens is utilized to acquire the high-resolution images of 4000 × 6000 pixels at regular intervals of a low-speed test. A test rate of 0.5 mm/min and a load frequency of 0.05 Hz is employed during static and fatigue tests respectively to maximize the high resolution of acquired images. The Ncorr open source 2D codes [24, 25] implemented in MATLAB is employed for the full-field post-processing DIC analysis of acquired images for different experimental tests, previously used in other work [20].

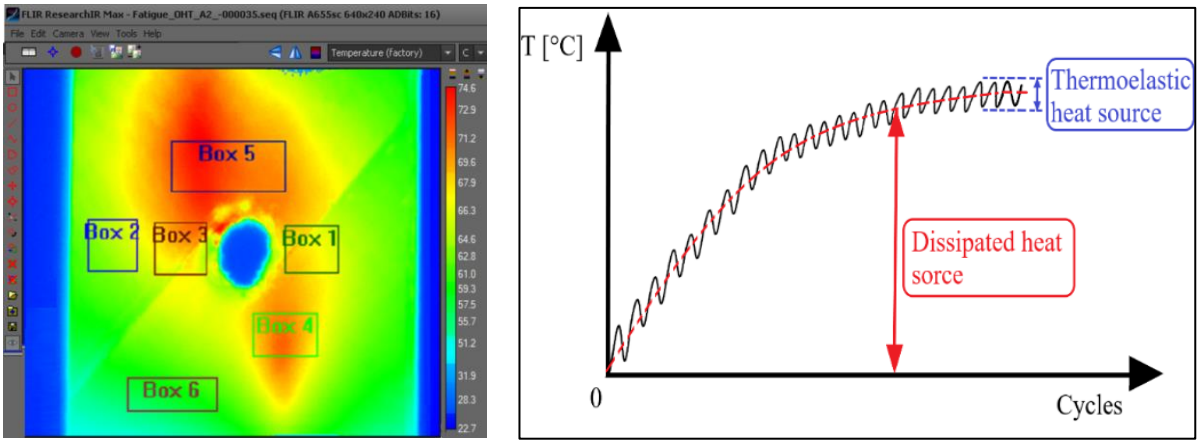

(a) (b)

Figure 3. (a) Thermal map at 69.6% of fatigue life for A3 coupon with ROIs; (b) schematic diagram of thermal behaviour during fatigue test.

In addition, non-destructive infrared thermographic (IRT) and ultrasonic (UT) tests are performed during suitable fatigue test interruption [19]. As example, the ND results for 5T sample are reported at 184,000 cycles (57.7 % of fatigue life) to allow UT and IRT inspections and check material state. Non-destructive evaluation employing pulsed thermography is done with the FLIR A655sc thermal imaging camera and a halogen lamp 1000 W. The IR technique provides a full-field inspection without sample removal from machine actuators. IR thermal acquisitions have a duration of about 150 seconds with a frame rate of 6.25 Hz and heating times of 20-30s is selected.

The UT inspections are performed with Omni-scan MX control unit employing a Phased Array OLYMPUS 2.25L64 probe with 64 transducers. A Plexiglas base was applied to the probe to optimize the wave beam between probe and sample surface with a coupling gel to ensure good transmission of the UT signal [20].

3. Results and discussion

3.1. TSA results

Preliminary compliance analysis is done for each fatigue test. Comparative analysis of stiffness behaviour as function of fatigue life is presented in Figure 4(a) for 'T-S' type and 'A' type elements. Stiffness data are normalized to specific maximum initial value (K_0) and show a clear different trend between the two-sample series, motivated mostly by different manufacturing process effects and load history.

In Figure 4(a), experimental data of 5T and 4T samples highlight a slow decreasing trend during initial and intermediate test phase, achieving a final stiffness degradation around 4 ÷ 8 % at 99% of fatigue life. Small *K* deviations are followed by a sudden decay before final failure. Specimen 3T results undamaged after the selected load (10^6 cycles) and damage absence obviously shows an almost flat stabilized trend with a slightly reduction of 2% of stiffness. The A2 sample, representative of 'A' series, presents significative stiffness degradation with a final reduction of 43 % at 99% of fatigue life. In this series, the 40% of total life seems to produce a compliance decrease around 7% with evident damages around the critical zone. After 60% of fatigue life, internal damage initiations seem to accelerate until final failure providing the collapse when internally the induced macro defects start to propagate through the whole specimen section. Thus, in the fatigue damage assessment composites, the classical approach based on compliance analysis confirms a robust reference for data evaluation.

As anticipated, fatigue damage initiation and failure prediction could be determined in terms of signal perturbations of raw thermal sequences or TSA processed data acquired during fatigue test [20].

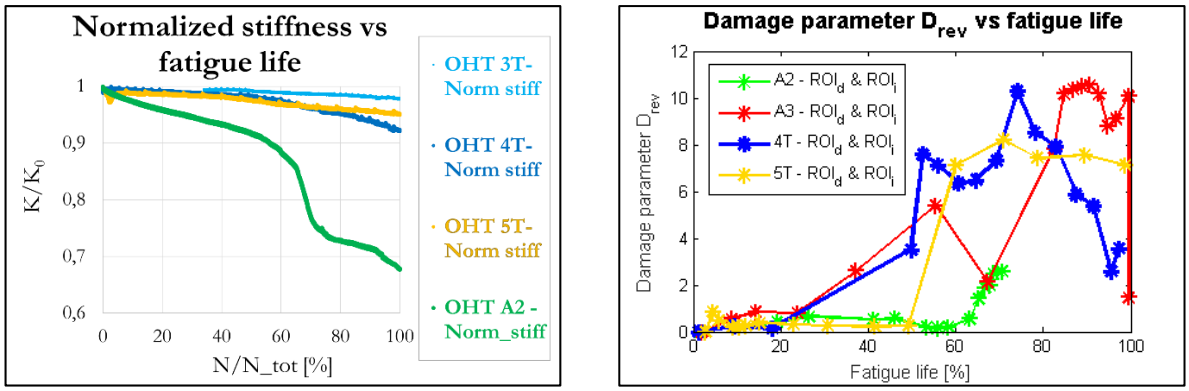

(a) (b)

Figure 4. (a) Normalized stiffness and (b) reversible damage D_{rev} vs fatigue life for OHT series.

In fact, thermographic approach could be successfully employed for damage monitoring, providing as output results from equations (4) and (5) that should result relate to thermoelastic effects to cyclic loads or to intrinsic energy dissipation. In Figures 4(b), 5(a) and 5(b), the processed thermal profiles of selected ROIs are reported for damage evaluation with stiffness degradation (D_K), reversible (D_{rev}) or dissipative heating (D_{diss}) sources during fatigue life respectively. The comparative analysis of damage parameters defined as Equation (4) and (5) provides different diagrams of TSA contrast data at different fatigue cycles for each sample series. Specific analysis ROIs are chosen for each specimen by maximizing the damage parameter were analysed. The intact area was calculated in several zones to evaluate the influence of ROI selection on damage factors values. In Figure 4(b), the D_{rev} data show high level of noise (scattering) and a certain trend variability due to ROI choice has been noted, but parameter values seem to increase in each specimen. It appears that D_{rev} behaviour follows the damage regime even if it suffers a lot of noise and critical damage propagation is clearly distinguished, highlighting similar behaviour between A3, 5T and 4T samples. In general, the D_{rev} parameter seems characterized by an initial phase, that starts form 20% of fatigue life without an evident growth of parameter trend, and by a second phase, where an evident curve growth over 1 seems to occur in all the specimens after 20% and at 50-55% life in 'A' and 'T-S' specimens' series, respectively.

In Figures 5(a) and 5(b), both diagrams show comparative analysis between damage diagrams evaluated with stiffness degradation (D_K) and behaviour with the dissipative thermal parameter (D_{diss}) profiles. D_{diss} data show a damage evolution with an approximately exponential trend with foible data variability. Even the variation of stiffness does not differ much from D_{diss} curves, which look very similar and common steep severe damage increase in case of A2 and A3 specimens manufactured via Infusion technique, whilst three autoclave produced samples show a damage behaviour more gradually increasing up to failure. In the first stage, thermal contrast profiles elaborated through D_{diss} parameter provide slight data variation due to internal micro-cracking between fibers and matrix and to damage nucleation that

begin to propagate in initial phases of fatigue test. In the next phase, the temperature reaches an almost stable increasement due to slow damage propagation and initial delamination, highlighting the different damage evolution between CFRP sample typology. Finally, this increasing trend is followed by a rapid contrast rise, leading to the final rupture. D_K and D_{diss} diagrams appear interlocking and intersecting each other, resulting in very similar correspondence and there is a better agreement between the proposed damage parameter D_{diss} and the stiffness measurement for all the specimens, even for the A2 sample for which we have not retrieved the final data.

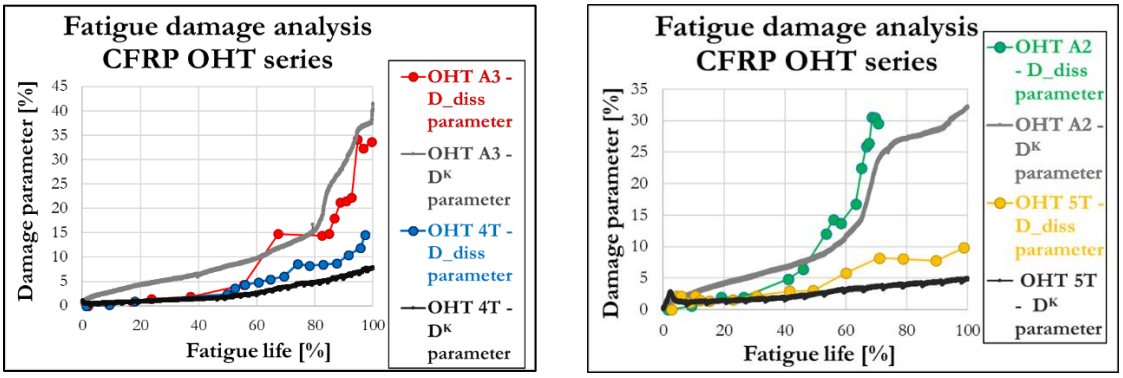

(a) (b)

Figure 5. (a) – (b) Comparative analysis between D_K and dissipative damage D_{diss} parameter vs fatigue life for OHT series.

Assuming initially undamaged conditions, the proposed damage parameter evaluated by D_{diss} data seems to provide an interesting comparable behaviour, as observed in cumulative damage D_K profiles related to stiffness degradation as function of fatigue life, validating initial assumptions on raw damage initiation proposal, based on TSA approach, and implemented according to a contrast-based method. This comparative analysis validates the new damage parameter definition previously described for realistic fatigue damage estimation using TSA contrast-based approach contained in the D_{rev} coefficient and the alternative thermal dissipation D_{diss} coefficient, proposed for damage propagation.

3.2. DIC analysis

In fatigue of composite materials, fibre-reinforced polymer composites are matrix cracking, fibre–matrix debonding, ply delamination and fibre breakage represent the most common failure mechanisms. The strain field on surface should provide important aspects of fatigue damage propagation prior to final failure in terms of displacement variations. Thus, the authors employ digital image processing to analyse strains and displacements for selected ROIs onto specimens, performed with Ncorr software implemented in MATLAB environment.

Six Virtual Extensometers (VE) of 16 ÷ 22 mm in length are selected for strain and displacement analysis in static and fatigue test cases. As shown in the example Figure 6(a), the employed VE consist of four extensometers parallel to applied load and the other two normal to load.

In Figure 6(b), the diagram shows the σ_y / ε_y trends of the VE-1 and VE-4 (located as shown in Figure 6(a)) for the residual strength test of 3T sample post fatigue cycles, where higher strain values are observed in the critical section at the countersunk zone. Specific ROIs are selected for different test cases for a proper evaluation in critical areas where maximum stress, displacements and strain concentration should be observed. In the first phase, the DIC analysis is carried out for the static test case (as seen in the 2.2 paragraph) in an area of interest relatively large area of around the hole zone. In the second phase, the DIC data acquired at the various regular intervals are evaluated during entire fatigue to estimate displacement and strain variation.

Figures 7 to 8 report an example comparative analysis the angular deformation γ_{xy} maps for 5T and A3 respectively at two three different instants (1% to 79% ÷ 88%), highlighting in both test a high strain state around the hole's zone and similar cross deformation state since test beginning. As damage seems to evolve during fatigue life, the strain values increase in the critical zones for a specific cyclic load, as

seen for the TSA results. As expected, in Figures 7, the γ_{xy} data of 5T shows an evident asymmetrical deformation state due to countersunk bolted joining caused by the load transfer through the bolted plates that may lead to higher strain levels.

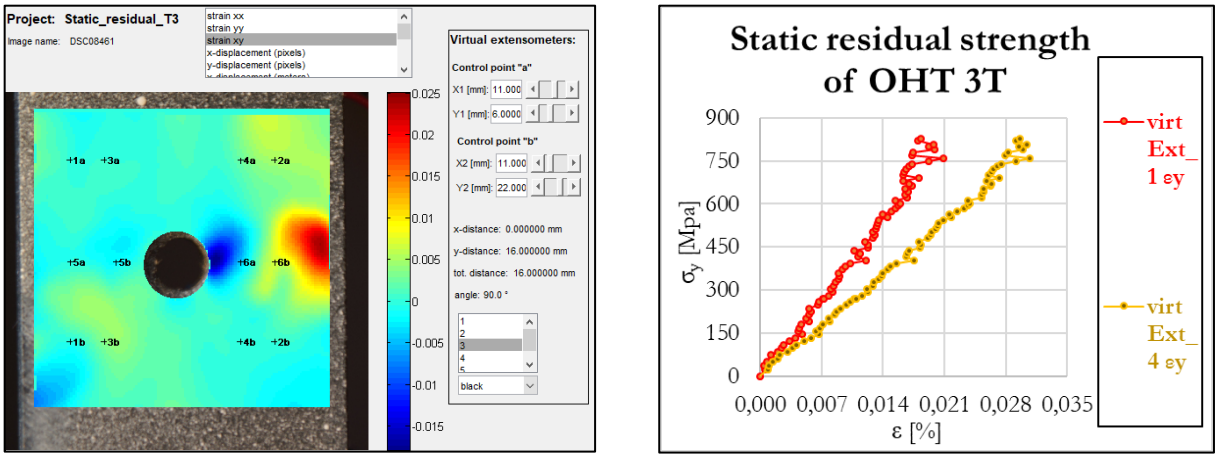

(a) (b)

Figure 6. (a) Angular deformation γ_{xy} map and (b) σ_y / ε_y diagram virtual extensometer VE-1 and VE-4 for residual strength test of 3T sample.

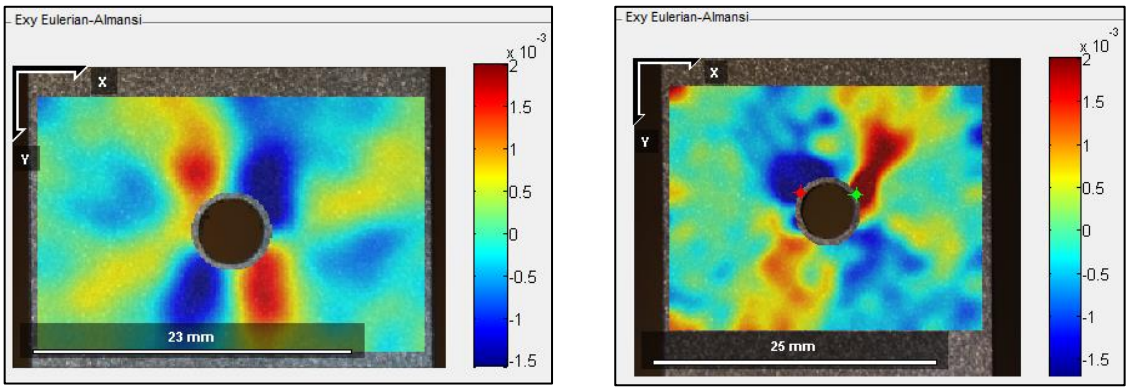

(a) (b)

Figure 7. (a) Angular deformation γ_{xy} maps at 1% vs (b) 88% fatigue life for 5T sample.

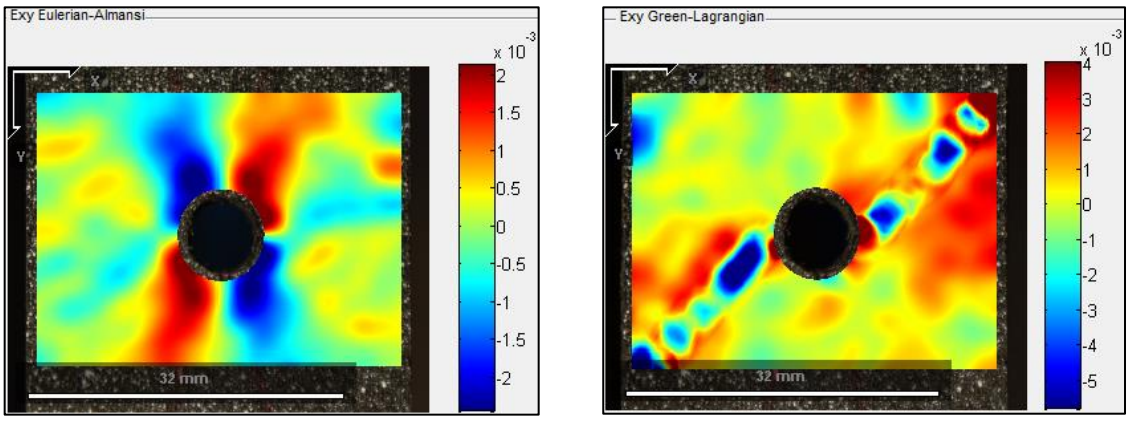

(a) (b)

Figure 8. (a) Angular deformation γ_{xy} maps at 1% vs (b) 79% fatigue life for A3 sample.

In Figures 8, higher deformation of critical section could be clearly observed in 'A' sample during cyclic test, along with shear coupling deformation along the fibre orientation of unidirectional first ply specimen. Therefore, the processed DIC images seem to establish complementary information also useful for a qualitative evaluation of damage initiation and location on inspected part during fatigue phases.

3.3. ND evaluation results

Figure 9(a) shows thermal distribution of 5T sample at 1.5 cooling seconds after a heating time of 20s carried out during short test interruption at 57.7 % of fatigue life, where the hottest zones seem to be localized in the middle section of specimen when final damage degradation arises, as described from D_{diss}/D_K parameters. As expected, the static ND evaluation highlights two widespread delaminations around the critical zone of countersink hole, as reported in Figure 9(a).

In previous works, the authors introduced a contrast-based (Local Boundary Contrast, LBC) algorithm implemented in a MATLAB GUI that avoids defining the free-defect zones when computing SNR, providing different contrast maps that highlights defective zones boundaries and location, as shown in Figure 9(b) [21].

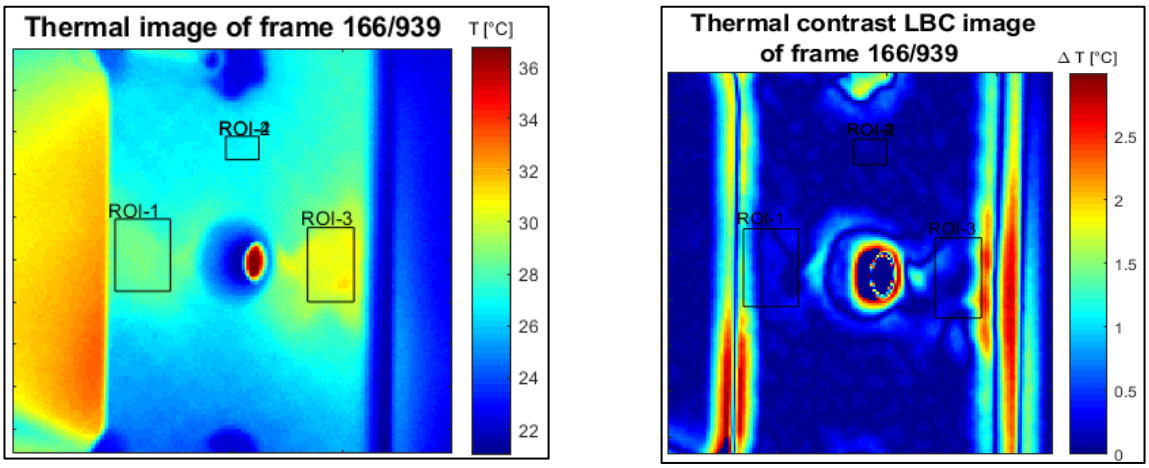

(a) (b)

Figure 9. (a) Thermal vs (b) LBC maps at 1.5 cooling seconds after a heating time of 20s of 5T sample.

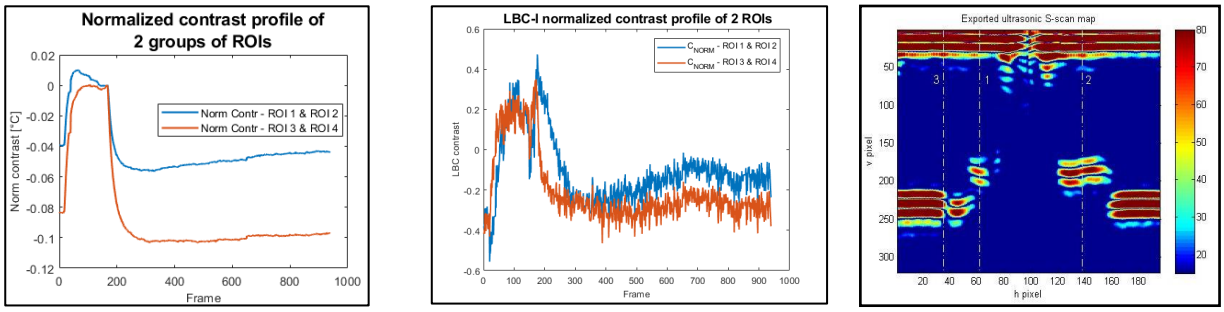

(a) (b) (c)

Figure 10. (a) Thermal vs (b) LBC contrast profiles and (c) S-Scan (0°) for post-fatigue 5T sample.

The same MATLAB GUI provide a manual selection of Region of Interest (ROIs) employed for a comparative analysis of normalized contrast evaluation of raw thermal data and LBC, as shown in Figures 10(a) and 10(b) respectively.

As shown in Figure 10(c), the post-fatigue damage on the reduced section is also qualitatively evaluated in the ultrasonic S-scan map, where the presence of both delaminations can be observed affecting the first plies from the side of the detached hole in accordance with TSA degradation of real-

time IRT signal detected during the fatigue test. Damage extension seems to be greater on right side compared to the left one, in perfect accordance with IRT data.

4. Conclusions

The composite damage initiation is not easy to be detected during fatigue tests before final failure. Therefore, in this proposed study the authors provide to perform a synergic and suitable combination of full-field monitoring methods for a possible damage analysis based on open hole CFRP specimens under cyclic loading.

The comparative analysis between the stiffness degradation and the post-processed thermal results obtained using TSA approach during fatigue tests is discussed for two batches of OHT elements, showing an interesting correlation between damage evolution evaluated with experimental results and TSA post-processed data. The comparative proposes a fatigue damage evaluation using TSA contrast-based approaches.

In addition, thermographic inspections highlight the presence of internal delamination after 57.7 % of fatigue life in perfect accordance with the well-established UT data.

5. References

[1] Vassilopoulos AP and Keller T 2011 Experimental Characterization of Fiber-Reinforced Composite Materials. In: Vassilopoulos AP, Keller T., editors. Fatigue of Fiber-reinforced Composites, Springer, 25 - 67.

[2] Subramanian S, Reifsnider K L and Stinchcomb W W 1995. A cumulative damage model to predict the fatigue life of composite laminates including the effect of a fibre-matrix interphase. *Int J Fatigue* 17 (5), 343 – 51. 10.1016/0142-1123(95)99735-S.

[3] Güemes A, Fernandez-Lopez A, Pozo A R and Sierra-Pérez J 2020 Structural Health Monitoring for Advanced Composite Structures: A Review, *J. Compos. Sci.*, **4**, 13, 10.3390/jcs4010013

[4] de Castro B A, Baptista F G and Ciampa F 2019 Comparative analysis of signal processing techniques for impedance-based SHM applications in noisy environments, *Mechanical Systems and Signal Processing* **126**, 326 – 340, 10.1016/j.ymssp.2019.02.034

[5] Middleton C A, McCrory J P, Greene R J, Holford K and Patterson E A 2019 Detecting and Monitoring Cracks in Aerospace Materials Using Post-Processing of TSA and AE Data, *Metals* **9** (7) 748, 10.3390/met9070748

[6] Rodrigues F de Sá, Marques R, Tabrizi I E, Kefal A, Qasim Ali H, Yildiz M and Suleman A 2021 A new methodology for thermoelastic model identification in composite materials using digital image correlation. *Opt and Las in Eng* **146** 106689

[7] Thatcher J, Crump D, Devivier C, Bailey P and Dulieu-Barton J 2020 Low cost infrared thermography for automated crack monitoring in fatigue testing, *Opt. Lasers Eng* **126** :105914

[8] Pitarresi G, Cappello R and Catalanotti G 2020 Quantitative thermoelastic stress analysis by means of low cost setups. *Opt. Lasers Eng* **134**: 10615

[9] Subramanian S, Reifsnider K L and Stinchcomb W W 1995. A cumulative damage model to predict the fatigue life of composite laminates including the effect of a fibre-matrix interphase. *Int J Fatigue* **17** (5), 343 – 51. 10.1016/0142-1123(95)99735-S.

[10] Toubal L, Karama M and Lorrain B 2006 Damage evolution and infrared thermography in woven composite laminates under fatigue loading. *Int J Fatigue* **28**, 1867 – 1872. 10.1016/j.ijfatigue.2006.01.013

[11] Chrysochoos A 2002 Infrared thermography, a potential tool for analysing the material behaviour. *Mécanique & Industries* **3** (1), 3-14.

[12] La Rosa G and Risitano A 2000 Thermographic methodology for rapid determination of the fatigue limit of materials and mechanical components, *Int J Fatigue* **22** (1), 65-73

[13] Galietti U, Demelio G P, Palumbo D and De Finis R 2016 A new rapid thermographic method to assess the fatigue limit in GFRP composites, *Compos B*. **103**: 60 - 67.

[14] Colombo C, Bhujangrao T, Libonati F and Vergani L 2019 Effect of delamination on the fatigue life of GFRP: A thermographic and numerical study. *Composite Structures* **218**, 152-161. 10.1016/j.compstruct.2019.03.023

[15] Ricotta M, Meneghetti G, Atzori B, Risitano G and Risitano A 2019. Comparison of Experimental Thermal Methods for the Fatigue Limit Evaluation of a Stainless Steel. *Metals* **9** (6): 677, DOI: 10.3390/met9060677
[16] Meneghetti G, Ricotta M and Pitarresi G 2019 Infrared thermography-based evaluation of the elastic-plastic J-integral to correlate fatigue crack growth data of a stainless steel. *Int J Fatigue* **125**, 149–160. 10.1016/j.ijfatigue.2019.03.034
[17] Fleuret J, Ebrahimi S, Ibarra-Castanedo C and Maldague X P V 2021 Independent Component Analysis Applied on Pulsed Thermographic Data for Carbon Fiber Reinforced Plastic Inspection: A Comparative Study May 2021 Applied Sciences. *Applied Sciences* **11**(10): 4377, 10.3390/app11104377.
[18] Vavilov V P and Burleigh D D 2015 Review of pulsed thermal NDT: Physical principles, theory and data processing. *NDT Int.* **73**, 28–52, 10.1016/j.ndteint.2015.03.003.
[19] Marzo F 2021 Analisi e monitoraggio del danneggiamento a fatica di provini CFRP aeronautici. *Master Thesis in Mechanical Engineering*, University of Salento, Lecce (73100).
[20] Dattoma V, Panella F, Pirinu A and Castriota A 2019 Fatigue damage on CFRP plates under bending by thermographic and UT analysis, aided with FEM-DIC prediction. *Pro Stru Inte* **24**, 978 – 987. 10.1016/j.prostr.2020.02.085.
[21] Dattoma V, Nobile R, Panella F, Pirinu A and Saponaro A 2018 Advanced NDT procedures and thermal data proceessing on CFRP aeronautical components. In Proceedings of the IRF 2018 of 6th International Conference Integrity-Reliability-Failure, Lisbon, Portugal, 22–26 July 2018.
[22] F. W. Panella and A. Pirinu 2021 Fatigue behaviour and damage evaluation on aeronautical CFRP elements under tension-tension and bending loads: two cases of study, *Int J Fatigue* **152** (13): 106403, 10.1016/j.ijfatigue.2021.106403.
[23] Galietti U, Demelio G P, Palumbo D, De Finis R 2017 Study of damage evolution in composite materials base on the Thermoelastic Phase Analysis (TPA) method, *Compos B* **117**, 49 - 60.
[24] Blaber J, Adair B and Antoniou A 2015 Ncorr: Open-Source 2D Digital Image Correlation Matlab Softwar,e *Exp. Mech*. **55** (6): 1105–1122, 10.1007/s11340-015-0009-1
[25] Nežerka V Antoš J, Sajdlová T and Tesarek P 2016 Use of Open Source DIC Tools for Analysis of Multiple Cracking in Fiber-Reinforced Concrete, *Appl Mech and Mater* **827**: 336 – 339, 10.4028/www.scientific.net/AMM.827.336

Acknowledgments
Authors would like to thank the Prof. U. Galietti for sharing the thermographic equipment and the student Francesco Marzo for his work in the experimental activities.